

# Anomalies in the superconducting dome of the Bi-cuprates

L. Dudy<sup>1,2</sup>, A. Krapf<sup>2</sup>, H. Dwelk, S. Rogaschewski<sup>2</sup>, B. Müller<sup>2</sup>, O. Lübben<sup>2</sup>, C. Janowitz<sup>2</sup>, and R. Manzke<sup>2</sup>

<sup>1</sup>*Randall Laboratory, University of Michigan, Ann Arbor, MI 48109-1040, USA*

<sup>2</sup>*Humboldt-Universität zu Berlin, Institut für Physik, Newtonstr.15, D-12489 Berlin, Germany*

(Dated: November 2, 2018)

We report characterization results by energy dispersive x-ray analysis and AC-susceptibility for a statistically relevant number of  $\text{Bi}_{2+z-y}\text{Pb}_y\text{Sr}_{2-x-z}\text{La}_x\text{CuO}_{6+\delta}$  single crystals. We show that the two structurally quite different modifications of the single-layered Bi-cuprate, namely  $\text{Bi}_{2+z-y}\text{Pb}_y\text{Sr}_{2-x-z}\text{La}_x\text{CuO}_{6+\delta}$  with  $y=0.4$  and  $\text{Bi}_{2+z}\text{Sr}_{2-x-z}\text{La}_x\text{CuO}_{6+\delta}$ , exhibit anomalies in the superconducting transition temperature at certain hole doping, e.g. at 1/8 holes per Cu. These doping values agree well with the 'magic doping fractions' found in the temperature dependent resistance of  $\text{La}_{2-x}\text{Sr}_x\text{CuO}_4$  by Komiya et al. [1]. This new set of findings suggests that all these anomalies are generic for the hole-doped high-temperature superconductors.

PACS numbers: 74.25.Dw, 74.72.Gh

## I. INTRODUCTION

One central paradigm in research of the hole-doped high-temperature superconducting cuprates (HTSC's) is the so-called 'generic phase-diagram', where the appearance of phases is shown in relation to the hole-doping and temperature. In this generic phase-diagram the superconducting dome, the superconducting transition temperature ( $T_C$ ) relative to the hole-doping, is typically illustrated as a flipped parabola which exhibits the maximum at around 16 percent holes per Cu atom. This parabola is called the 'universal curve' [2] and is suggested to be universal for all HTSC materials. The differences in the various HTSC-materials are accounted for by commonly scaling this parabola, in most cases just by scaling to maximum  $T_C$ . In one very practical application, an appropriately scaled parabola can then be used for straightforward estimation of a samples' hole-doping. This estimation is often done especially in the Bi-cuprates where the doping can hardly be determined exactly.

Beside the practical aspect of having a simple and smooth parabola, there is also the possibility that there are generic anomalies of  $T_C$  within the superconducting dome. There seems to be at least one certain hole-doping value where  $T_C$  shows an anomaly and is suppressed. Historically, the first anomaly found was in  $\text{La}_{2-x}\text{Ba}_x\text{CuO}_4$  (LBCO) at a hole-doping value of 1/8 by Moodenbaugh et al. [3]. Also  $\text{La}_{2-x}\text{Sr}_x\text{CuO}_4$  (LSCO) has a 1/8 anomaly, but additionally, other fractional anomalies (so called 'magic doping fractions') can be suggested for this material [1, 4]. Komiya et al. [1] extracted for the hole-doping of these the relation  $p=(2m+1)/2n$ , where  $p$  is the hole-doping and  $m$  and  $n$  are integers. In order to complete the list of known anomalies,  $\text{YBa}_2\text{Cu}_3\text{O}_{7-x}$  (YBCO) shows also a reduction in  $T_C$  which was found quite early and is often referred to as 'the 60K plateau' [5]. This '60K plateau' can be associated with 1/8 hole-doping value [6]. There also exists a '90K plateau' in YBCO. For the Bi-cuprates, there is less knowledge about the ex-

istence of a 1/8 anomaly or others. There is only one report for  $\text{Bi}_{2+z}\text{Sr}_{2-x-z}\text{La}_x\text{CuO}_{6+\delta}$  by Yang et al. [7]. It might therefore be interesting to examine members of the Bi-cuprates for these anomalies. In the case that a Bi-cuprate also shows anomalies at the same doping values like the other HTSC's, it can be suggested that the simple parabola is only a zeroth order approximation and an included finer structure is generic for the HTSC's.

A generic existence of anomalies may also rely on important and interesting physics which prominently shows up in the numerous studies in connection with the 1/8 problem. Essentially, the experiments indicate spin and charge-order within the  $\text{CuO}_2$ -plane [8–11] resulting in more insulating behavior [1, 3] accompanied by a large single particle gap at the antinodes [12] as well as the suppression of Josephson coupling perpendicular to the planes [13]. From a theoretical point, among many models proclaimed so far, there exist some models which account for some, if not all, findings about the 1/8 anomaly. In the phenomenological view, examples for these possibilities are, at least, the two formulations of so-called pair-density waves [14–16]. For the microscopic picture, these phenomenological formulations might be respectively broken down to the existence of a Wigner-like-crystal of Cooper pairs [14] or the formation of stripes [15, 16]. Another microscopic model which might be relevant here is that of a Wigner-like crystal of holes in an antiferromagnetic background [17, 18].

All these mentioned models have in common that they not only aim to explain superconductivity but also account for the existence of, at least, a 1/8 anomaly. Thus, there might be insights to gain by examining not only the superconductivity of the HTSC's but also its absence. So it comes that the present manuscript aims to discuss that members of the Bi-cuprate exhibits anomalies of  $T_C$  at certain hole-dopings, similar to the ones found by Komiya et al. [1]. Shown here are results from single crystals of the one-layers  $\text{Bi}_{2+z}\text{Sr}_{2-x-z}\text{La}_x\text{CuO}_{6+\delta}$  (La-Bi2201) and  $\text{Bi}_{2+z-y}\text{Pb}_y\text{Sr}_{2-x-z}\text{La}_x\text{CuO}_{6+\delta}$  ((Pb,La)-Bi2201). The process of hole-doping in the Bi-cuprates is quite complex: In  $\text{Bi}_{2+z}\text{Sr}_{2-z}\text{CuO}_{6+\delta}$  (Bi2201), the hole doping

is done by extra oxygen and the amount of Bi on Sr positions, whereas in La-Bi2201 the hole doping can be controlled by lanthanum substitution only. Additionally substituting Pb on Bi positions, i.e. (Pb,La)-Bi2201, leads with high enough amount of Pb to structurally more clean crystals. These crystals are dominantly in the so-called ' $\beta$ -phase' (see, e.g., [19]) which means that these crystals are free of an incommensurate quasi 1x5 superstructure. Since Pb is an active dopant and the extra oxygen ( $\delta$ ) is known to be reduced by Pb substitution (see, e.g., [20]), the same lanthanum content will produce different hole-dopings in both systems (see [21]).

The organization of this manuscript is as follows. First, we will show by a statistically relevant amount of characterization data that in both of these systems, La-Bi2201 and (Pb,La)-Bi2201, anomalies of  $T_C$  exist at certain, but different, La concentrations. This will be done by applying a refinement scheme that first uses the full data obtained from 299 crystals and then reduces the number of samples by defining restrictions, which are meant to optimize the superconducting properties or 'cleanness' of these materials. As both do show anomalies but at different La content, this already suggests that the anomalies found cannot be a feature of the La substitution but only depend on the hole doping value. For LSCO, the existence of anomalies will be shown from a collection of data from the literature. In LSCO, under correct annealing conditions, the hole concentration is merely directly proportional to the strontium substitution level. Therefore, the La concentrations of the anomalies in La-Bi2201 and (Pb,La)-Bi2201 can be assigned to a hole-doping value according to the hole concentrations of the anomalies in LSCO. Eventually, a scaling between the La- (and implicitly the Pb-) content relative to the hole-doping is constructed. This hole-lanthanum scaling equals perfectly the scaling obtained by x-ray absorption spectroscopy (XAS) [21, 22]. Because the opposite direction can be argued, it is therefore shown that also in the two single-layer Bi-cuprates anomalies at certain hole dopings exist. This suggests that all HTSC's exhibit anomalies at always the same hole dopings.

## II. SUPERCONDUCTIVITY IN RELATION TO THE LANTHANUM AND LEAD CONTENT

Single crystals of (Pb,La)-Bi2201 were grown by the self-flux method; details were reported elsewhere [19]. The samples were characterized by energy dispersive x-ray analysis (EDX) and AC-susceptibility. EDX probes the chemical composition for each crystal and is computed standard-free by the use of the PUzaf-correction [23]. To compute the elementary composition for Cu, the K doublet was used. For La and Sr, the L-series was used and for Bi and Pb the M series. By AC-susceptibility, we obtain  $\chi'$  and  $\chi''$  which are respectively the real and imaginary parts of the AC-susceptibility times the volume of the sample and a filling factor. For the measure-

ments, a commercial Quantum Design PPMS 6000 system with 0.1 Oe as the amplitude of the magnetic field was used. The AC-susceptibility for a (Pb,La)-Bi2201 single crystal is presented in the inset of FIG. 1. The real part  $\chi'$  indicates an onset- $T_C$  of 36 K and a transition range ( $\Delta T_C$ ) of 3 K. The transition range is derived from the temperature range using the criterion that the real part changes in a 90 to 10 percent range from the paramagnetic to the superconducting state.

The whole dataset contained 299 crystals which were optically selected for smoothness and regular shape. Superconducting samples were chosen with the restriction that only one peak in the imaginary part of their AC-susceptibility is present. Initially, no distinction was made between a small or broad transition width as long as the peak in the imaginary part is Gaussian-like and the real part downturn is smooth.

The chemical composition obtained by EDX was then fitted by a linear dependence. For this, the Pb content ( $y$ ) and the La content ( $x$ ) were assumed to be independent of each other. If the content of Bi, Sr and Cu is written as  $c(\text{Bi})$ ,  $c(\text{Sr})$  and  $c(\text{Cu})$ , the linear dependencies of these 299 samples are given by

$$\begin{aligned} c(\text{Bi}) &= (2.08 \pm 0.01) - (0.21 \pm 0.01)x - (1.12 \pm 0.01)y, \\ &\chi^2 = 0.70246; \\ c(\text{Sr}) &= (1.79 \pm 0.01) - (0.78 \pm 0.01)x + (0.12 \pm 0.01)y, \\ &\chi^2 = 0.55005; \\ c(\text{Cu}) &= (1.13 \pm 0.01) - (0.01 \pm 0.01)x + (0.01 \pm 0.01)y, \\ &\chi^2 = 0.60479. \end{aligned}$$

In order to define a clean phase, we apply a refinement scheme which we call here the 'compositional restriction'. For this restriction, crystals with a deviation of the Bi, Sr or Cu composition from the linear dependencies larger than 0.05 formula units were removed. By applying this restriction, the size of the dataset was reduced to 208 samples.

In the upper (a) panels of FIG. 1, the chemical composition of Bi, Sr and Cu versus the lanthanum content is shown. The resulting  $T_C$  relative to the Lanthanum content for the compositional restricted dataset is shown in the lower (b) panels of FIG. 1. There, the data are shown in slices of the Pb content, for  $y=0$ ,  $y \in ]0;0.3]$ , and  $y \in ]0.3;0.6]$ . It is clearly indicated that the maximum achievable superconducting transition temperature  $T_C^{max}$  increases by increasing the amount of Pb. Typically, the curve  $T_C$  vs La content is described as a parabolic curve (see, e.g., [24]), but here the data points appear strongly scattered or irregular although the dependence of Bi, Sr, and Cu vs the lanthanum content looks smooth. For Pb concentrations higher than  $y=0$ , this can be best observed when looking at the Bi curve and the Pb curve, which have to be complementary in their gradients and curvatures when Pb substitutes for Bi. For  $y=0$ , a strong scattering of  $T_C$  values takes place in the region around  $x=0.25$ , 0.4, and 0.6 formula units. At  $y \in ]0;0.3]$ , no definitive values can be found because the statistics are

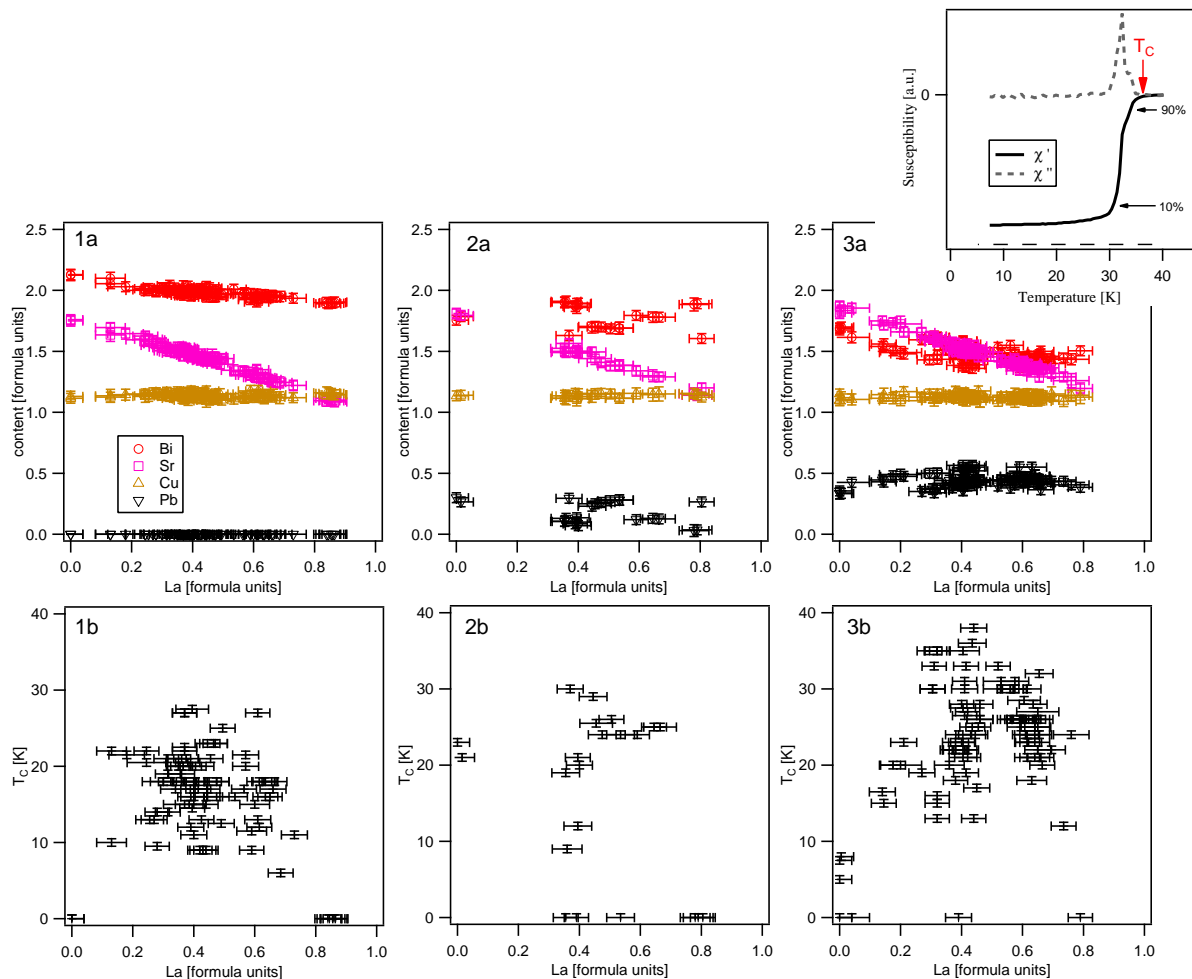


FIG. 1: Characterization results of the  $\text{Bi}_{2+z-y}\text{Pb}_y\text{Sr}_{2-x-z}\text{La}_x\text{CuO}_{6+\delta}$  single crystals as obtained by energy dispersive x-ray analysis (EDX) and AC-susceptibility. The inset in the upper right shows a typical AC-susceptibility result and the definitions used: The superconducting transition temperature is the onset- $T_C$ , the transition width  $\Delta T_C$  is the temperature range where the real part of the susceptibility drops from 90% to 10% from the paramagnetic state into the diamagnetic state. The top panels 1a, 2a and 3a display the results of the EDX characterization. Shown is the average chemical composition of Bi, Sr and Cu vs the average lanthanum content. Panel 1a shows this for Pb-free samples ( $y=0$ ), whereas Panel 2a shows this for the low Pb-content of  $y \in [0;0.3]$  and Panel 3a for the high Pb-content of  $y \in [0.3;0.6]$ . The lower panels show the  $T_C$  as obtained by AC-susceptibility vs the average lanthanum content  $x$ . Panel 2a shows this for  $y=0$ , Panel 2b for  $y \in [0;0.3]$  and Panel 3b for  $y \in [0.3;0.6]$ .

quite poor. It is suggested that there is a center of scattering around  $x=0.4$  formula units. For  $y \in [0.3;0.6]$ , a strong scattering is visible in the region of  $x=0.4$  and  $0.65$  formula units. We will see that this scattering is not accidentally but that these regions contain anomalies.

### A. Anomalies in $T_C$

The large number of data points makes it possible to apply some statistical routines to gain a deeper insight into the true three-dimensional  $T_C$  vs La and Pb phase diagram. First, one can average over all crystals of particular composition, which may act to remove effects of

a variation of the extra oxygen  $\delta$  and other experimental uncertainties. The averaging algorithm used and described in the APPENDIX A, relies on a Gaussian probability distribution and includes all experimental uncertainties. FIG. 2 shows the averages from that dataset which was before refined by the compositional restriction. Three selected cuts are shown given by the restrictions  $y=0$  (a),  $y=0.4$  (b), and  $x=0.4$  (c), respectively. Also shown in this figure are the individual datapoints which were used to compute this average. These are marked by light gray crosses. The average  $T_C$  curve for fixed La upon the change in the Pb substitution, as shown in FIG. 2 (c), indicates clearly an overall trend of an increase in  $T_C$  by increasing the amount of Pb. It is suggested that

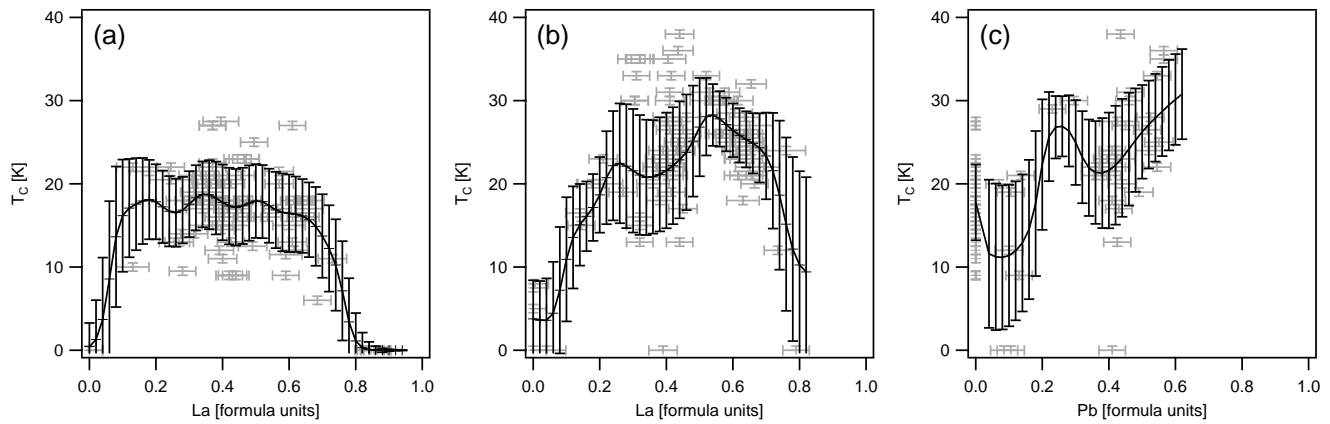


FIG. 2: Averaging the  $T_C(x,y)$  values of the  $\text{Bi}_{2+z-y}\text{Pb}_y\text{Sr}_{2-x-z}\text{La}_x\text{CuO}_{6+\delta}$  single crystals. The averaging algorithm relies on a Gaussian probability distribution (see APPENDIX A). The continuous curve in all three panels is the averaged  $T_C(x,y)$ , plotted here for  $y=0$  (a),  $y=0.4$  (b) and  $x=0.4$  (c). Also indicated is the standard deviation for the averaging. The light gray crosses are the original data-points  $T_C(x,y)$  as also shown in FIG.1.

the irregularity between 0 and 0.3 formula units of lead has its origin in a strong phase-mixture as discussed by Luebben et al. [19]. Thus, there exists a Pb substitution region in the  $\text{Bi}_{2+z-y}\text{Pb}_y\text{Sr}_{2-x-z}\text{La}_x\text{CuO}_{6+\delta}$  system where the superconducting properties might be strongly influenced by the competition of two different structural phases. However, samples without Pb and samples with high Pb content ( $>0.3$ ) are then either dominantly in one phase or the other. This is, why we will discuss only the series with  $y=0$  and  $y=0.4$ . These are shown in FIG. 2 (a) and (b), respectively. From the averaged  $T_C$  for  $y=0$  (a) and  $y=0.4$  (b), a strictly parabolic-like curve is still not found. Instead, there are reductions or anomalies of  $T_C$ . These take place for the Pb-free series at La concentration of  $x \approx 0.25 \pm 0.02$ ;  $0.43 \pm 0.02$  and  $0.58 \pm 0.02$  formula units. For  $y=0.4$ , an anomaly can be seen at  $x \approx 0.4 \pm 0.02$  and  $0.62 \pm 0.02$  formula units and possibly at  $x \approx 0.28 \pm 0.04$ . But, because of the high variance, the conclusion of a finer structure within the parabolic curve may yet be unconvincing. Therefore, we will establish more arguments on statistical grounds.

In the following analysis, we will prominently regard samples without Pb. This is merely because there are more data from this concentration than for  $y=0.4$  and therefore the statistical argument will weight stronger. The dataset in this  $y=0$  region, filtered by the compositional restriction, contains 82 samples. One interesting question is whether the form of the averaged curve of FIG. 2 (a) is strongly dependent on the chosen ensemble. Whether the ensemble is representative or not can, of course, never be determined. We can only apply the following philosophy: The 'compositional restriction' applied before convinced us that the chemical composition is well defined as the dependence of Bi, Sr, and Cu versus the lanthanum content is smooth. Variations of the hardly controllable excess oxygen can be averaged out. Now, more restrictions can be performed to maybe

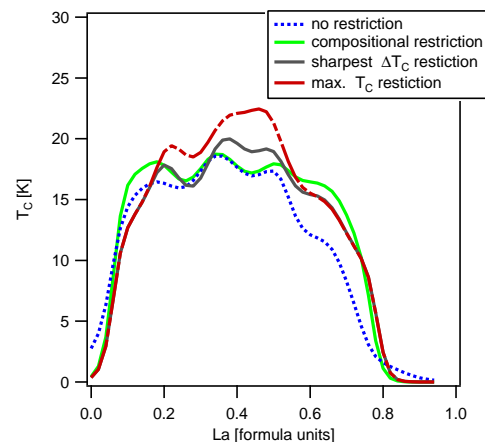


FIG. 3: Reducing the number of crystals in order to optimize the superconducting properties. Here, the averaged  $T_C$  for several changes in the ensemble is compared: There is the average of the dataset without any restriction (dotted line), the dataset with the compositional restriction (solid line), the 'sharpest'  $\Delta T_C$  reduced dataset (dark gray solid line) and the 'maximum  $T_C$ ' reduced dataset (dashed line). These 'maximum  $T_C$ ' reduced dataset and 'sharpest'  $\Delta T_C$  reduced dataset were performed by choosing the samples with the highest  $T_C$  or sharpest  $\Delta T_C$  in its lanthanum 'slot' or interval of 0.02 formula units. One can see that the curves change but show always anomalies (suppressions of  $T_C$ ) at about the same lanthanum level.

further optimize the superconducting properties of the dataset. These restrictions will reduce the magnitude of our ensemble and make it possible to test for changes, i.e. whether the anomalies persist in the  $T_C$ -curve or not. For this further refinement, we tested two slightly different criteria. One is called here the 'sharpest  $\Delta T_C$ '-criterion while the other one is the 'maximum  $T_C$ '-criterion. The idea behind this sharpest  $\Delta T_C$ -criterion is

that one large contribution to the transition width  $\Delta T_C$  comes from the level of uniformity for the composition on the scale of the coherence length, whose scale is in the tenth of an Angstrom. This suggests that from samples, with the same composition measured by EDX, the sample with a sharper transition width is structurally better than the sample with a broader transition; It has a better compositional uniformity below the scale of the typical area measured by EDX, which is typically on the micron scale. Thereby, it might be that by this restriction such samples have the best superconducting properties. A similar argument can be used to justify the maximum  $T_C$ -criterion which is taking always that sample with the highest  $T_C$  from the multitude of samples with the same composition. Technically, first the compositional restriction is applied. Then, these additional criteria are applied, by selecting either that sample with the lowest transition width  $\Delta T_C$  or with the highest  $T_C$  compared to the other samples present in the same La-content 'slot'. The slots had a width of  $\Delta x = 0.02$  formula units. Each of these two restrictions reduces thereby the dataset to 27 samples. After applying these restrictions, the individual data points are averaged. The result of this process is shown in FIG. 3. where the averaged  $T_C$  for the sharpest  $\Delta T_C$ -criterion reduced dataset can be compared to the dataset with only the compositional restriction. Also shown is the averaged  $T_C$  for the maximum  $\Delta T_C$ -criterion reduced dataset. It is interesting to see that the curve from samples with the maximum  $T_C$  is not the same as the one with the sharpest  $\Delta T_C$ . Finally also shown is the averaged  $T_C$  for all characterized samples without applying any restrictions. For comparison, this dataset contains 139 samples. What can clearly be seen in FIG. 3 is that all the La- $T_C$ -curves change slightly but *always* show anomalies at almost the same lanthanum concentrations.

### III. CONSIDERATION OF THE HOLE CONTENT

The methods for determining the exact value of the hole content of the  $\text{CuO}_2$ -plane in Bi2201 shall be briefly discussed. For, e.g.,  $\text{La}_{2-x}\text{Sr}_x\text{CuO}_4$  (LSCO), the method to determine the hole-content is relatively straight forward. Under correct annealing conditions (see, e.g., [25]),  $\text{La}_{2-x}\text{Sr}_x\text{CuO}_{4+\epsilon}$  has nearly a stoichiometric amount of oxygen. Therefore, merely determining the value of the Sr-content  $x$  gives the hole content  $p$ . In the Bi2201 system, the situation is more complicated. One reason is that measuring the quite low concentrations of extra oxygen in tiny single crystals is an experimentally formidable task. In the publication of Ando et al. [24], the hole content in single crystals was estimated by comparing the normalized Hall-coefficient of La-Bi2201 to LSCO. The authors give the dependence  $p=0.21-0.13x$  for La-Bi2201 in the substitution range  $0.23 < x < 0.84$ . A second method to consider the hole-content is by the ratio

between the  $\text{Cu-L}_{III}$  white-line and the  $\text{Cu-L}_{III}$  charge transfer satellite. These quantities can be obtained and analyzed in an x-ray absorption spectroscopy (XAS) experiment. For polycrystalline La-Bi2201 and (Pb,La)-Bi2201, this method was applied by M. Schneider et al. [22]. The hole scale there differs from the scaling determined by the comparison with the normalized Hall coefficient by Ando et al. [24]. From the XAS measurements, the relation is given as  $p=0.24-0.21x$  for La-Bi2201, and  $p=0.23-0.22x$  for PbLa-Bi2201. It should be noted here that the Pb-substituted ceramics had a large unsystematic variation in the Pb-content. Also for single-crystals, despite an unusual in-plane polarization dependence [26], the scaling could be obtained by XAS [21]. The crystals used there had a more defined Pb substitution level as the ceramics of Schneider et al. [22]. The scaling of the hole-concentration relative to the La-content for PbLa-Bi2201 with  $y \simeq 0.4$  was evaluated in the single crystals as  $p=(0.23 \pm 0.02)-(0.16 \pm 0.05)x$ .

In the following, we will perform a comparison method to consider the hole-content. For this, we first will discuss a collection of  $T_C$  data for LSCO from the literature from which we will show that anomalies of  $T_C$  are present in LSCO. Thus, we have the hole concentrations of anomalies in LSCO and we have the La-content of anomalies from the series without lead and with lead substitution of  $y=0.4$  formula units. Eventually, by assigning the hole-value of anomalies found in LSCO to the La-values of the anomalies found in La-Bi2201 and PbLa-Bi2201, we can thereby construct a hole scaling for the number of holes in La-Bi2201 and PbLa-Bi2201. Then, we are able to discuss the resulting hole scaling in relation to the hole-scales as given in the literature [21, 22, 24] and also discussed above.

#### A. Anomalies of $T_C$ in LSCO

$T_C$  values for LSCO were obtained by resistivity measurements and are taken from [1, 27–36]. This collection is shown in the upper left panel of FIG. 4. Also depicted is the averaged  $T_C$  versus  $p$  curve for all the 98 data points. To generate the curve, four additional data points at  $p=0.27, 0.28, 0.29,$  and  $0.30$  with  $T_C=0$  were used. These extra points are used to improve the visualization and can be justified in that for  $p > 0.26$ , no superconductivity is detectable. The most remarkable feature of the  $T_C$  vs  $p$  curve is that it is also not a simple parabola for LSCO. This can be seen compared to the 'universal curve', which is also depicted in the figure and calculated for  $T_C^{max} = 40$  K. At certain doping concentrations, an anomaly of  $T_C$  occurs. The first derivative of the averaged  $T_C$  vs  $p$  curve is shown on the upper right panel of FIG. 4. These anomalies can be seen as maxima of  $\partial T_C / \partial p$ . Due to the fact that, in the literature, typically the maximum  $T_C$  achievable is given and due to the assumption of a Gaussian distribution in the averaging algorithm, these singularities are slightly smeared

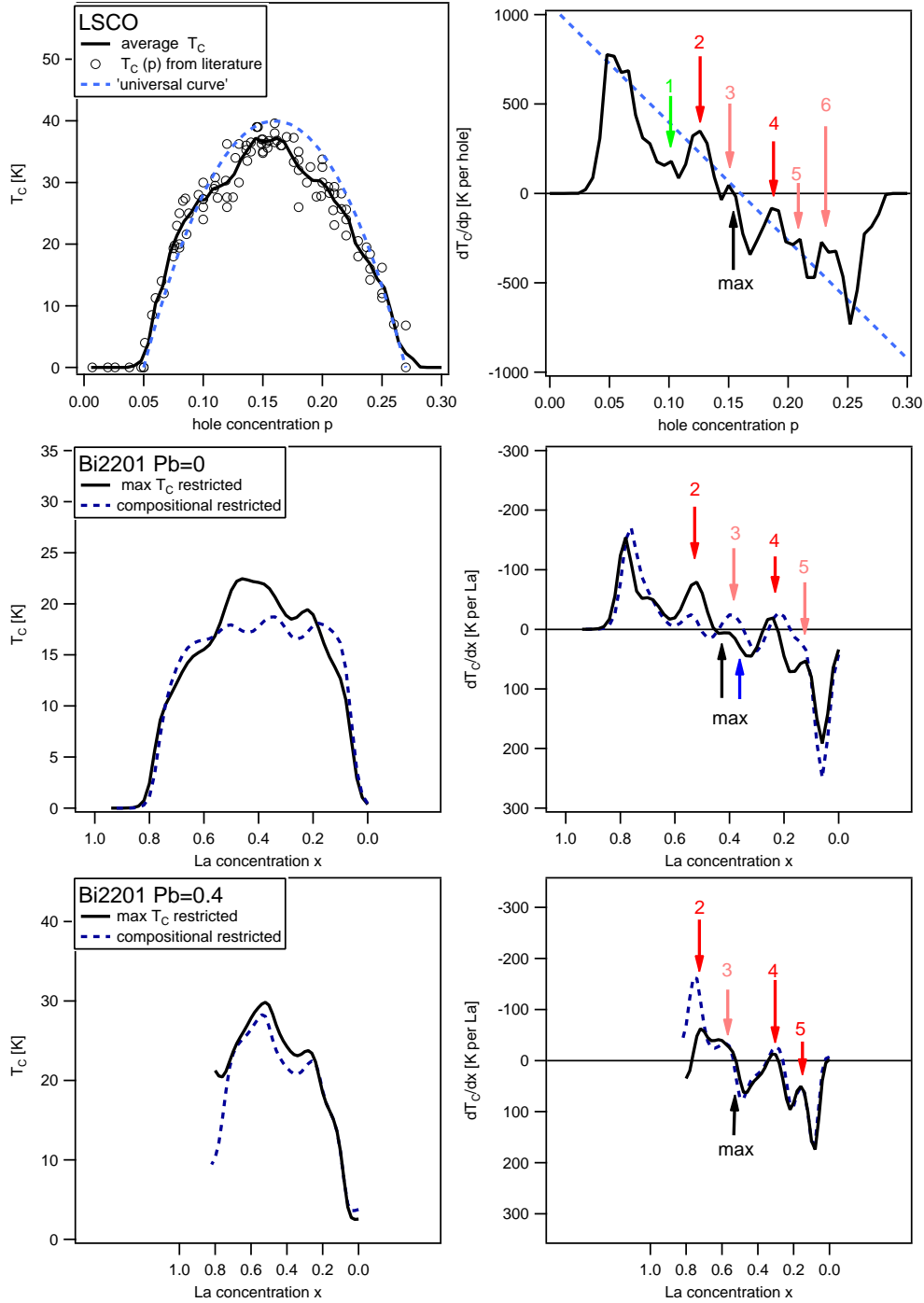


FIG. 4: The upper Left panel shows the experimental  $T_C$  and hole doping values for LSCO as compiled from the literature [1, 27–36]. The solid line is the averaged curve derived within this work for all the 98 experimental data points. The dashed curve represents the 'universal curve', computed with the maximum transition temperature  $T_C^{max}=40\text{K}$ . The upper right panel shows the first derivative of the average  $T_C$  vs hole-concentration ( $p$ ). The anomalies of  $T_C$  at hole dopings of about  $x=0.1$ ,  $0.125$ ,  $0.15$ ,  $0.185$ ,  $0.21$ , and  $0.235$  are marked by arrows. The dashed line is the derivative of the 'universal curve'. The panels below show the average  $T_C$  vs lanthanum concentration curves for  $\text{Bi}_{2+z-y}\text{Pb}_y\text{Sr}_{2-x-z}\text{La}_x\text{CuO}_{6+\delta}$  for the Pb contents of  $y=0$  (middle left panel) and  $y=0.4$  (lower left panel). The derivatives of these averaged  $T_C$  curves are shown respectively on the right panels. The maximum  $T_C$ -restricted average is the solid line and the compositional restricted average is the dashed line. The assignment of the anomalies is indicated in all right panels by arrows; Also included is the maximum position of the  $T_C$  curve. Please compare also with TAB. I.

description	label of the maxima of the 1st. derivative						$T_C^{max}$ position
	1	2	3	4	5	6	
LSCO x [holes/Cu] †	0.98	0.126	0.15	0.188	0.21	0.228	0.156
magic fractions [1]	3/32	1/8	5/32	3/16	7/32	15/64	-
as floats:	0.094	0.125	0.156	0.188	0.219	0.234	-
	La content x [formula units]						
La-Bi2201 comp. restr. ‡	-	0.54	0.39	0.22	0.14	-	0.44
La-Bi2201 max. $T_C$ restr. ‡	-	0.53	0.41	0.25	0.13	-	0.36
(Pb,La)-Bi2201 y=0.4 comp. restr. ‡	-	0.75	0.58	0.30	0.16	-	0.53
(Pb,La)-Bi2201 y=0.4 max. $T_C$ restr. ‡	-	0.72	0.58	0.31	0.16	-	0.52

TABLE I: From top to bottom: The doping of the anomalies found in LSCO. The 'magic doping fractions' [1] given by the formula  $p=(2m+1)/2n$  where  $m$  and  $n$  are integers. The positions in La content of the depressions found in (Pb,La)-Bi2201 for the different averaging methods. On the right column, the  $T_C^{max}$  position of every curve is written.

† error estimated as  $\pm 0.005$  holes/Cu.

‡ for individual error estimation please compare with FIG. 5.

out. In the upper right panel of FIG. 4, the anomalies are marked by arrows. They occur at hole dopings of approximately  $p=0.098$ , 0.126, 0.15, 0.188, 0.21 and 0.228 holes per Cu.  $T_C^{max}$  is reached at a doping of about 0.156 holes per Cu. The error is estimated at about  $\pm 0.005$  holes per Cu. The anomalies at  $p=0.098$ , 0.15, 0.21 and 0.228 are weaker and the exact positions more uncertain, while the anomalies at  $p=0.126$  and 0.188 are more pronounced. The bounce visible in the  $T_C$  curve, and also in the derivative as an upturn around 0.26, is due to the additionally inserted non-experimental data points described above. However, it is worth noting that all these anomalies are very well known, e.g. one anomaly of  $T_C$  occurs at hole concentrations of  $1/8$  [3]. The other anomalies agree with the 'magic doping fractions' found by Komiya et al. [1].

## B. Scaling by the anomalies

As shown earlier, the Bi2201 crystals used here also exhibit anomalies. These are visible in the  $T_C$  vs La curve and can be used to scale the hole concentrations. This scaling is, of course, based on the assumption that these anomalies must occur at the same doping concentrations as those for LSCO. In addition to the derivative of the average  $T_C$  vs hole concentration curve for LSCO, FIG. 4 shows the derivatives of the average  $T_C$  vs lanthanum concentration curves for  $\text{Bi}_{2+z-y}\text{Pb}_y\text{Sr}_{2-x-z}\text{La}_x\text{CuO}_{6+\delta}$  for the Pb contents of  $y=0$  and  $y=0.4$ . Please note that the La-scale is reversed compared to the hole-scale of LSCO, as substitution of divalent strontium by trivalent lanthanum reduces the amount of holes. The averages used for the derivatives are the compositionally-restricted average, which is the data first refined by the compositional restriction only and then averaged, and the 'maximum  $T_C$ -restricted average'. The maximum  $T_C$ -restricted average is the data first refined by the compositional restriction, then refined by the maximum  $T_C$  criterion and then averaged. The maximum  $T_C$ -restricted

average is used because it might better resemble the features produced by a resistivity measured  $T_C$ -curve. This is because, in the case of heterogeneous samples, by resistivity the path with the highest  $T_C$  will be probed. The maxima of the derivative of the average  $T_C$ -curve of Bi2201 were assigned to these anomalies. This assignment is simply by counting the 'peaks' in the derivatives from the position of  $T_C^{max}$  at about 16% hole-doping. In the right side of FIG. 4, the positions of the  $T_C^{max}$  in the derivatives are marked by blue or black arrows and labeled 'max'. The assignment of the 'peaks' is also indicated by arrows in FIG. 4 and also listed in TAB. 1.

FIG. 5 shows the lanthanum concentration of the maxima of the first derivative for both restricted averages vs the assigned anomalies. This assignment enables us now to construct a lanthanum-hole scaling. In agreement with Schneider et al. [22] and Ando et al. [24], we assume a linear behavior for the lanthanum-hole scaling. This assumption can be justified by a rather small  $\chi^2$ -value found. A linefit yields the following relations for the Pb content  $y=0$ :

$$p_c = (0.23(6) \pm 0.01) - (0.20(9) \pm 0.02)x, \text{ and}$$

$$p_m = (0.23(9) \pm 0.01) - (0.21(4) \pm 0.01)x.$$

The first scaling relation, with  $p_c$ , is the linefit for the maxima of the first derivative for the compositionally-restricted average which was the dataset refined by the compositional restriction only and then averaged. The corresponding averaged curve is the dashed line in the middle panels of FIG. 4 and the maxima of this curve are marked by squares on right panel of FIG. 5. The second scaling relation, with  $p_m$ , is the linefit for the maxima of the first derivative for the maximum  $T_C$ -restricted average which was that what was first refined by the compositional restriction and then -additionally- by the max- $T_C$  criterion and then averaged. The corresponding averaged curve is the solid line in the middle panels of FIG. 4 and the maxima of this curve are marked by squares on left panel of FIG. 5. In both these relations,  $p$  is given in holes per Cu and  $x$  is in formula units. Please note the

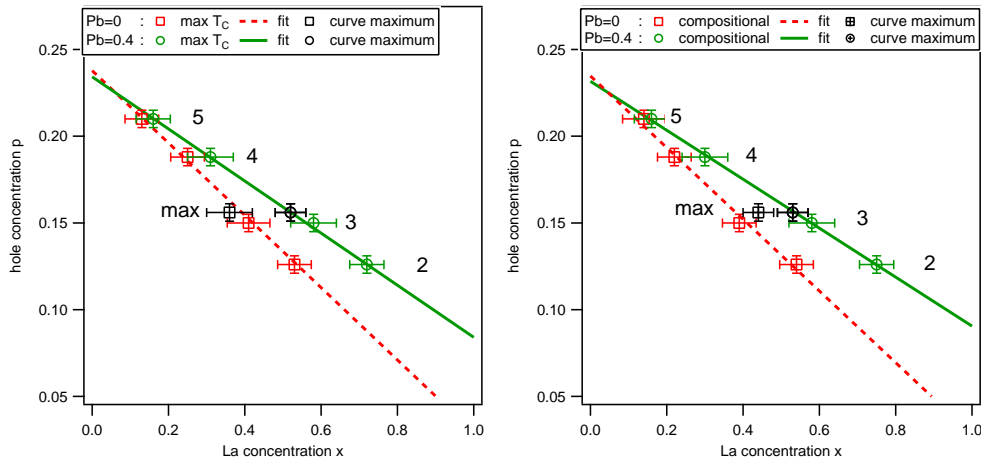


FIG. 5: The lanthanum concentration of the maxima in first derivatives for both restricted averages vs the hole doping of the maxima found in LSCO. Please compare with TAB. I. On the left side, the maximum  $T_C$  restricted average is shown for Pb content of  $y=0$  (boxes) and  $0.4$  (circles). On the right side, the same is done for the compositional-restricted average. Also, the positions of the maximum transition temperature ( $T_C^{max}$ ) for  $y=0$  and  $y=0.4$  and both averages vs the  $T_C^{max}$  position in LSCO are shown. Also included are the linefits for the four restricted averages.

perfect agreement with the measurements in Schneider et al. [22]. For Pb content  $y=0.4$ , the relations are

$$p_c = (0.23(2) \pm 0.01) - (0.14(1) \pm 0.01)x, \text{ and}$$

$$p_m = (0.23(4) \pm 0.01) - (0.14(8) \pm 0.01)x.$$

Again, the first scaling relation, with  $p_c$ , is the linefit for the maxima of the first derivative for the compositionally-restricted average. The corresponding averaged curve is the dashed line in the lower panels of FIG. 4 and the maxima of this curve are by circles on right panel of FIG. 5. The second scaling relation, with  $p_m$ , is the linefit for the maxima of the first derivative for the maximum  $T_C$ -restricted average. The averaged curve is the solid line in the lower panels of FIG. 4 and the maxima of this curve are by circles on left panel of FIG. 5. Here, the measurements do not concur as well with Schneider et al. [22]. As already mentioned, the discrepancy might have its origin in the unsystematic variation of Pb content there. The agreement with the more Pb-homogenous single crystals used by Ariffin et al. [21] is good.

In FIG. 6, finally, the  $T_C$  vs hole concentration curves achieved by this scaling are shown. The scaling used is the fit from the max.  $T_C$  average (pm). The left side of FIG. 6 shows the scaling of the max.  $T_C$  average of  $\text{Bi}_{2+z-y}\text{Pb}_y\text{Sr}_{2-x-z}\text{La}_x\text{CuO}_{6+\delta}$  for Pb content  $y=0$  whereas the right side shows the same for the  $y=0.4$  series. Also included for Pb content  $y=0$  is the comparison with the scaling and data of Ando et al. [24]. For both Pb concentrations, the averaged  $T_C$ -curve for LSCO and the 'universal curve' are also shown. With respect to LSCO and the 'universal curve', the curve for  $\text{Bi}_{2+z-y}\text{Pb}_y\text{Sr}_{2-x-z}\text{La}_x\text{CuO}_{6+\delta}$  with Pb content  $y=0$  shows a faster drop at the underdoped and overdoped sides. The same trend is obvious for the  $y=0.4$  result of FIG. 6 although the final conclusion may suffer from the

limited data set.

#### IV. DISCUSSION

In this publication, we showed that the superconducting transition temperature for  $\text{Bi}_{2+z-y}\text{Pb}_y\text{Sr}_{2-x-z}\text{La}_x\text{CuO}_{6+\delta}$  with  $y=0.4$  and  $\text{Bi}_{2+z}\text{Sr}_{2-x-z}\text{La}_x\text{CuO}_{6+\delta}$  exhibit anomalies at certain lanthanum concentrations. A hole scaling was achieved by assigning the anomalies visible in the  $T_C$  vs lanthanum graph to certain dopings. This assignment gives the same hole doping vs lanthanum scaling derived with x-ray absorption spectroscopy by Schneider et al. [22] and Ariffin et al. [21]. It is suggested that the difference in the scaling-relation for Bi2201 derived here and by Schneider et al. [22] compared to the scaling derived in [24] is due to a difference in crystal growth, the method of determining the chemical composition and the differences in methods for obtaining the hole-concentrations. In fact, analyzing the  $T_C(p)$  data of Ando et al. [24], as reproduced on the left side of FIG. 6, there is a change in curvature at around 0.14 to 0.15 holes per Cu which we attribute to  $1/8$ . Rescaling the hole-doping vs lanthanum equation of [24] with this knowledge and the knowledge that  $T_C^{max}$  is at around a lanthanum level of 0.4 does not yield our hole-doping vs. lanthanum scaling. Unfortunately, we found it impossible to estimate possible compositional differences other than the lanthanum between our crystals and the crystals of Ando et al. [24]. Differences might be, for example, in the Bi-Sr exchange. However, as here the same scaling was achieved by either a direct quantitative method [21, 22] and additionally by a comparison method, the hole-concentration curve presented here is validated, at least for crystals with similar chemical composition and



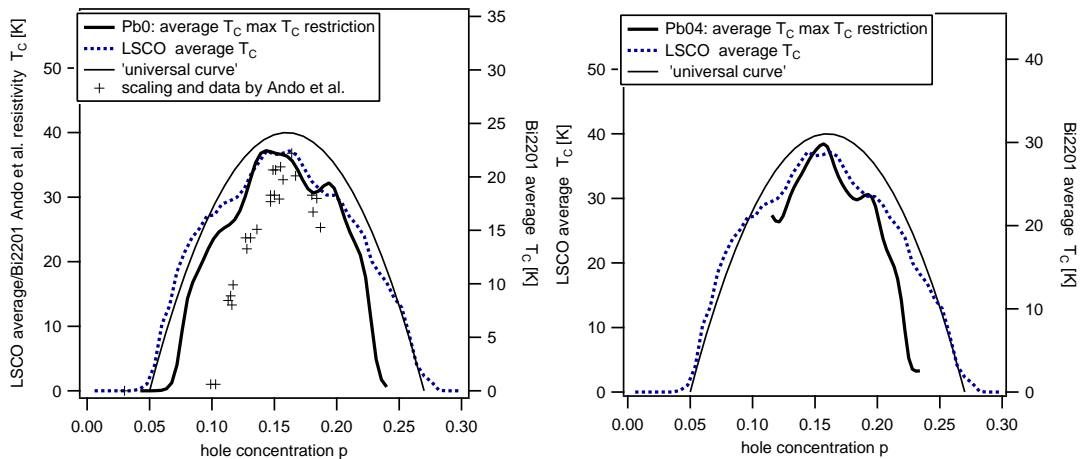


FIG. 6: Lanthanum hole scaling by the fit from the maximum  $T_C$  average (pm). Left for  $\text{Bi}_{2+z}\text{Sr}_{2-x-z}\text{La}_x\text{CuO}_{6+\delta}$ . There also included is the comparison with the scaling and data from Ando et al. [24]. Right for  $\text{Bi}_{2+z-y}\text{Pb}_y\text{Sr}_{2-x-z}\text{La}_x\text{CuO}_{6+\delta}$  with Pb content  $y=0.4$ . For both graphs the  $T_C$ -curve for LSCO and the 'universal curve' are also shown.

this composition obtained by a similar EDX processing.

In the course of this manuscript, we derived a hole-doping scale by an assignment of the La-value of the anomalies to the corresponding hole-values found for LSCO. Using the hole-scaling of Schneider et al. [22] and Ariffin et al. [21], we can turn the line of argumentation and then say that two kinds of Bi-cuprates show anomalies at very much the same hole-doping values as they are in LSCO. These extracted dopings of the anomalies agree with the 'magic doping fractions' found in LSCO by Komiya et al. [1]. There, the anomalies were measured as maxima in the normal-state (or pseudogap-state) resistivity. Here, we showed that with a large enough amount of data, the anomalies can be seen directly in the  $T_C(p)$  curve - without using high temperature signatures like it was done by Komiya et al. [1]. But, it is worth to mention that our resistivity measurements of the ab-plane also confirm a more insulating behavior at the anomalies. It is suggested that the identification of the anomalies by its high temperature signatures is possible due to the intimate relation between the anomalies and the pseudogap state. However, this issue is beyond the scope of this publications and will be addressed elsewhere.

By the last paragraph, we hope to have made clear that, in our view, the existence of a multitude of anomalies of  $T_C$  is proved for two-and-a-half cuprate systems: LSCO and two variants of Bi2201. The 'half' is related to the already mentioned fact that, with large enough amount of Pb, the Bi2201 crystals are dominantly in a different structural phase (see, e.g., [19]). We can next discuss the question whether the cause of these anomalies is a structural effect. For this, let us look at the following three facts: (1) The  $\text{CuO}_2$ -plane in  $\text{Bi}_{2+z-y}\text{Pb}_y\text{Sr}_{2-x-z}\text{La}_x\text{CuO}_{6+\delta}$  with  $y=0.4$  exists in a different structural environment than in  $\text{Bi}_{2+z}\text{Sr}_{2-x-z}\text{La}_x\text{CuO}_{6+\delta}$ . (2) The structural environment of  $\text{La}_{2-x}\text{Sr}_x\text{CuO}_4$  is quite different from both of

the Bi-cuprates. (3) The amounts of dopant-atoms for reaching optimal doping are very much different in all the three systems (La-Bi2201 (Pb,La)-Bi2201 and LSCO). Following this line of argumentation, structural effects can play no major role here. Also, for La-Bi2201 and PbLa-Bi2201, by the observation of the anomalies at different La-contents but the same hole-dopings, variations in the hole-doping due to the variation of the poorly controlled excess oxygen can be ruled out as a cause. In fact, the effect of the oxygen was already removed by our statistical Ansatz and the variation of the ensemble shown here. This statistical Ansatz seems generally beneficial - also for LSCO, where the hole-doping is better controllable than in the Bi-cuprates. The derived average  $T_C$  decreases at an anomaly, but it seems to us that the tendency of having a somewhat different  $T_C$  increases, a behavior which we can also slightly detect in the standard deviation of our averaging (see FIG.2). It is also an interesting question, whether this tendency of having somewhat different  $T_C$ 's is caused somehow by the mechanism of superconductivity in the  $\text{CuO}_2$ -plane itself or an indirect effect due to another parameter not well controlled or a combination of both. For the influence of a not well controlled parameter, an example is the 60K plateau in YBCO, the 1/8 anomaly [6], which can be reduced by ordering of the oxygen within the  $\text{CuO}$ -chains of the charge reservoir (please compare with [6, 37, 38]). Finally, another interesting question is why some anomalies, like 1/8 and maybe 5/32, seem to be more pronounced than others. A quantitative measure of this might be the different heights of the 'peaks' appearing in the derivative of the  $T_C$  curve (FIG. 4 right column).

Let us now discuss possible mechanisms causing these anomalies. For this, we review some experimental findings, mostly related to the 1/8 anomaly, and some theoretical concepts:

It is known that neutron scattering detects four-

fold superlattice peaks indicating a spatial spin-ordering [8, 9, 39]. X-ray-diffraction [10] and resonant soft x-ray scattering [11] also indicates charge ordering. A study for LBCO by angular resolved photoemission and scanning tunneling spectroscopy [12] showed that at 1/8 the d-like single particle gap shows a maximum. In  $\text{La}_{1.6-x}\text{Nd}_{0.4}\text{Sr}_x\text{CuO}_4$ , neutron scattering revealed [8] the superlattice peaks being commensurate with the underlying lattice. Assuming that this commensurability for  $\text{La}_{1.6-x}\text{Nd}_{0.4}\text{Sr}_x\text{CuO}_4$  is a typical sign at 1/8. In this case, one idea might be that at 1/8 are static (or commensurate) stripes (for a review see, e.g., [40]). Thus, there is a formation of hole-rich, quasi-one dimensional 'rivers of charge' separated by antiferromagnetic domains - an idea which has its roots in the mean-field results of Zaanen and Gunnerson [41]. In order to have this unidirectional order consistent with neutron scattering four-fold symmetry, there must be two domains rotated 90 degree to each other, most preferentially there is a stacking with the stripes rotated by 90 degree for each neighboring  $\text{CuO}_2$ -planes. However, unlike dynamical (or incommensurate) stripes, Emery et al. [42] stated that commensurability leads to a charge gap and insulating behavior which competes with superconductivity. There can be a commensurability effect within a stripe, which tends to pin when  $2k_F=2\pi/m$ , where  $m$  is an integer and  $k_F$  the Fermi-wavevector. There is also a commensurability effect between stripes. In the most conventional form, one can think of half-filled commensurate stripes which occur at hole-dopings  $p=1/2n$ . Here,  $n$  is an integer representing the spacing between the stripes.

Motivated by a pattern found in the power spectral density of topological data of scanning tunneling microscopy (see [43] and references therein), another relevant model might be the pair-density wave state (PDW-1) as described by Chen et al. [14]. When looking at the mean field result of an SO(5) model with extended interactions, it is found that there are insulating phases at fractional filling factors where Cooper pairs of the holes form a lattice which is usually commensurate with the underlying lattice. Thus, there is a phenomenological state where a non-vanishing superconducting order can coexist with a charge density wave order. These insulating PDW-1 states are a consequence of strong pairing and low superfluid density. By assuming a 'Law of Corresponding States', it can be predicted that these insulating PDW-1 states appear in the background of superconducting states at rational fillings of  $p=(2m+1)/2n$  [1]. Here,  $p$  is the hole-doping and  $m$  and  $n$  are integers. Let us point out that, unlike the static stripe scenario above, the order in the  $\text{CuO}_2$ -plane is two-dimensional. However, the existence of these PDW-1 states is dependent on the strength of an interaction parameter. There are therefore materials which are believed to show no anomalies, one example being  $\text{Bi}_{2+z}\text{Sr}_{2-z}\text{CaCu}_2\text{O}_{8+\delta}$  (Bi2212) [14]. By the construction principle, there is also a hierarchy of these PDW-1 states, where 1/8 is the most pronounced and most common anomaly followed equally

by the more uncommon 3/16 and 1/16 anomalies and so on (see [1]).

Another concept is that there is Wigner-crystallization of holes in an antiferromagnetic background as Kim and Hor [17, 18] deduced by analyzing far-infrared reflectivity measurements. At the hole-values of the anomalies and below the crystallization temperature an insulating hole-lattice is formed which is pinned to the underlying lattice, and therefore commensurate with it. Extra carriers (holes) occupy the interstitial sites and can 'ride' the Wigner lattice forming an 'interstitial band'. These extra carriers form spin-singlet Cooper pairs because they experience the negative dielectric screening in the frequency region between the Goldstone mode (in this situation, the phononic mode of the Wigner crystal) and the plasma frequency of the hole-lattice. Unfortunately, these ideas seem not to have triggered much further theoretical considerations. One may find it interesting to compare the picture of an 'interstitial band' with calculations on the Hubbard-Wigner model, for example exact diagonalization results for a finite size lattice [44] or results by single-site dynamical mean field theory [45]. It is also interesting that, in a (true) Wigner crystal, path-integral Monte Carlo calculations [46] do show strong attractive interaction between point defects. We would like to emphasize that, of course, in these correlated systems a crystallized hole-lattice with point defects in an antiferromagnetic background has some more constraints as just those given by the confinement on a lattice, an onsite-exchange interaction and long-range Coulomb interactions. That is because the Zhang-Rice singlet picture breaks down above  $p=0.25$  holes per Cu when nearest neighbor singlets would then have to share a mutual oxygen (compare with [47, 48]). However, for the doping values of the anomalies, Kim and Hor [18] expect them at  $p = m/n^2$  with nonzero integers  $m$  and  $n$  where  $m < n^2$ .

For LBCO, it seems to be that the onset of charge and spin order leads to the suppression of Josephson coupling between neighboring  $\text{CuO}_2$ -planes [13, 49]. In underdoped LSCO, it was shown that, when applying a moderate magnetic field  $H\parallel c$ , the interlayer coupling is suppressed albeit the in-plane superconducting properties remain intact [50]. The model of the 'striped superconductor' [15, 16] seems to be especially suitable to explain these experimental findings as it leads easily to the so-called 'dynamical layer decoupling' because the average  $c$ -axis Josephson-coupling vanishes. In this model, there is a time reversal invariant state in which the superconducting order parameter has a finite wave vector and changes sign over half a period. This state is confusingly also called a pair-density wave (PDW-2) but with a different meaning than for the one of Chen et al. [14]. While for PDW-1 the (non-vanishing) superconducting order parameter coexists with the order parameter of the charge density wave, for PDW-2 the average value of the superconducting order parameter vanishes and there is a charge density wave order induced with half the period of the modulation of the superconducting order parame-

ter. Going now from the phenomenological picture to a microscopical view [16], there is the picture of a superconducting striped state where neighboring stripes are antiphase in terms of the superconducting order parameter. In a layered system and with perfect stripe order within the planes, the antiphase superconducting order is able to greatly reduce the interplane Josephson couplings without the suppression of the antinodal gap. While the layer decoupling effect can be expected to be most pronounced where perfect stripe order is near  $1/8$ , it also occurs for some range about  $1/8$ . Another major difference of this model compared to the others discussed above is that before the anomalies were commensurate with the underlying lattice. In this PDW-2 model, there is no such commensurability and it is not as important as it is for the idea of static stripes, which was the first model reviewed here. A problem with static stripes is that, on the one hand, neutron scattering gives for  $1/8$  lower width of the superlattice peaks and there seems to be a saturation in the doping dependency of the superlattice peak's periodicity at  $1/8$  [51], but, on the other hand, in most of the nominal  $1/8$  samples of various HTSC's, the fourfold superlattice peaks are not interpreted to be originating from static stripes but dynamical ones. Often, within the view of stripes, the term 'quasi-static stripes' is used for this lack of perfect commensurability. In this view of the PDW-2 state, it might be a question whether commensurability is playing a major role in the  $1/8$  problem.

In order to discuss possible causes for not only  $1/8$  but for all the anomalies, we may say that all the theoretical models discussed above for  $1/8$  might be generally relevant but the weighting of some details may favor one or the other model. One criterion might be that for models favoring a unidirectional order, like the PDW-2 state of Berg et al. [15, 16], it might be more challenging to explain the other anomalies found - i.e. others than at  $1/8$ . Our derived values for the anomalies were quite similar to those of Komiya et al. [1], which suggests a two-dimensional order of some kind. On the other hand, this PDW-2 model explains the dynamical layer decou-

pling quite well, which is where the PDW-1 state of Chen et al. [14] seems to have a problem. A coexistence of charge-order and superconducting-order would generally reduce  $T_C$  and not leave the in-plane superconducting properties intact. However, this PDW-1 model reproduces quite well the doping values of the anomalies. As the deviation of the doping values of the anomalies with  $p=(2m+1)/2n$  is essentially by a two-dimensional geometrical construction scheme, we have some hopes that something similar may also apply to a model much like the single hole Wigner crystallization model of Kim and Hor [17, 18].

In summary, we showed that there are anomalies of  $T_C$  in La-Bi2201 and (Pb,La)-Bi2201 at certain hole-dopings. These hole-dopings agree well with the extracted 'magic doping fractions' found in LSCO by Komiya et al. [1]. In addition, from a collection of data taken from the literature, we showed for LSCO that with a large enough amount of data the anomalies can also be seen directly in the  $T_C(p)$  curve. This, together with the knowledge of the  $1/8$  anomaly in LBCO and YBCO, allows us to point to the strong possibility that *all these anomalies are generic for the hole-doped high-temperature superconductors*. The need to include these generic anomalies of  $T_C$  should help to privilege, expand or create theories which eventually will explain the occurrence of superconductivity in these materials.

#### A. Acknowledgement

We gratefully thank R. Müller, J. Röhler, E. Fradkin and J.W. Allen for valuable discussions during preparation of this publication. We thank M. Mioduszewski for critical reading of the manuscript. L.D. thanks J.W. Allen for his kind hospitality during finishing of this manuscript. We thank D. Kaiser for helping us greatly with the digitalization of the characterization list.

### Appendix A: Gaussian slotting algorithm

Here, we briefly describe the used averaging algorithm. The advantage of the algorithm is that non equispaced data can be used and that the data is weighted by its error. As usual, we write the chemical composition of La as  $x$  and the chemical composition of Pb is  $y$ . For the La-Pb phase diagram there are existing the non-equispaced continuous sampled dataset of the form  $T_C^j(x^j, y^j)$ , where  $j = 0, 1, \dots, (J - 1)$  is the indice of the  $J$  measured samples. As a result of the EDX measurement, we have a standard error for the composition,  $\sigma_x^j$  and  $\sigma_y^j$ . It contains the systematic error of EDX due to the fitting process and the statistical error from probing multiple areas on the samples' surface. From the multitude of these non-equispaced and continuous  $T_C^j(x^j, y^j)$ , we want to construct an equispaced discrete averaging function, here formally written as  $\overline{T_C}(p\Delta x, q\Delta y)$ . This can be done by weighting each  $T_C^j(x^j, y^j)$  with its standard error into each 'slot' ( $p\Delta x, q\Delta y$ ). Here,  $p = 0, 1, \dots, (P - 1)$  and  $q = 0, 1, \dots, (Q - 1)$  are the indice of the

slot. The averaging reads

$$\overline{T_C}(p\Delta x, q\Delta y) = \frac{1}{Z(p\Delta x, q\Delta y)} \int_{p\Delta x - \Delta x/2}^{p\Delta x + \Delta x/2} dx' \int_{q\Delta y - \Delta y/2}^{q\Delta y + \Delta y/2} dy' \sum_{j=0}^{J-1} \frac{T_C^j(x^j, y^j)}{2\pi\sigma_x^j\sigma_y^j} \times \exp \left\{ -\frac{(x' - x^j)^2}{2(\sigma_x^j)^2} - \frac{(y' - y^j)^2}{2(\sigma_y^j)^2} \right\}.$$

Here  $Z$  is the probability distribution and given as

$$Z(p\Delta x, q\Delta y) = \int_{p\Delta x - \Delta x/2}^{p\Delta x + \Delta x/2} dx' \int_{q\Delta y - \Delta y/2}^{q\Delta y + \Delta y/2} dy' \sum_{i=0}^{J-1} \frac{1}{2\pi\sigma_x^i\sigma_y^i} \exp \left\{ -\frac{(x' - x^i)^2}{2(\sigma_x^i)^2} - \frac{(y' - y^i)^2}{2(\sigma_y^i)^2} \right\}.$$

It is easy to see that the normalization makes sense:

$$\sum_{p, q=-\infty}^{\infty} Z(p\Delta x, q\Delta y) = J \approx \sum_{p, q=0}^{(P-1)(Q-1)} Z(p\Delta x, q\Delta y).$$

The largest error in this approximation comes from boundary effects of samples with  $x - \sigma_x < 0$  or  $y - \sigma_y < 0$ . Without loosing too much accuracy, for  $\Delta x, \Delta y \ll \sigma_x, \sigma_y$  the integrals above can be reduced to

$$\overline{T_C}(p\Delta x, q\Delta y) \approx \frac{\Delta x \Delta y}{Z(p\Delta x, q\Delta y)} \sum_{j=0}^{J-1} \frac{T_C^j(x^j, y^j)}{2\pi\sigma_x^j\sigma_y^j} \times \exp \left\{ -\frac{(p\Delta x - x^j)^2}{2(\sigma_x^j)^2} - \frac{(q\Delta y - y^j)^2}{2(\sigma_y^j)^2} \right\}.$$

The probability reads then after reduction

$$Z(p\Delta x, q\Delta y) \approx \Delta x \Delta y \sum_{i=0}^{J-1} \frac{1}{2\pi\sigma_x^i\sigma_y^i} \exp \left\{ -\frac{(p\Delta x - x^i)^2}{2(\sigma_x^i)^2} - \frac{(q\Delta y - y^i)^2}{2(\sigma_y^i)^2} \right\}.$$

These both approximations above were used for computing the averaged  $T_C$ -function. This averaging function is expected to be asymptotical unbiased as long as the estimated function, i.e. the true  $T_C$  function by hypothetically measuring an infinite fine doping series of perfect samples, is analytically and harmless. It is clear, that the variance of this averaging increases for slots with a low probability, i.e. with 'no samples in the slot'. For visualization of  $\overline{T_C}(p\Delta x, q\Delta y)$  it is therefore good to define a cutoff value. Below this value the function is not plotted. Therefore, it should be that

$$Z(p\Delta x, q\Delta y) \geq Z^{\text{cutoff}} := \frac{1}{2PQJ}.$$

From the normalization given above it can be seen that this means that half a samples probability has to be located in the slot.

- 
- [1] S. Komiya, H. D. Chen, S. C. Zhang, and Y. Ando, Phys. Rev. Lett. **94**, 207004 (2005).  
[2] M. R. Presland, J. L. Tallon, R. G. Buckley, R. S. Liu, and N. E. Flower, Physica C **176**, 95 (1991).  
[3] A. R. Moodenbaugh, Y. Xu, M. Suenaga, T. J. Folkerts, and R. N. Shelton, Phys. Rev. B **38**, 4596 (1988).  
[4] F. Zhou, P. H. Hor, X. L. Dong, W. X. Ti, J. W. Xiong, and Z. X. Zhao, Physica C: Superconductivity **408-410**, 430 (2004), ISSN 0921-4534.  
[5] R. J. Cava, B. Batlogg, C. Chen, E. A. Rietman, S. M. Zahurak, and D. Werder, Nature **329**, 423 (1987).  
[6] J. L. Tallon, G. V. M. Williams, N. E. Flower, and C. Bernhard, Physica C **282**, 236 (1997).  
[7] W. L. Yang, H. H. Wen, and Z. X. Zhao, Phys. Rev. B **62**, 1361 (2000).  
[8] J. M. Tranquada, B. J. Sternlieb, J. D. Axe, Y. Nakamura, and S. Uchida, Nature **375**, 561 (1995).  
[9] K. Yamada, C. H. Lee, Y. Endoh, G. Shirane, R. J. Birgeneau, and M. A. Kastner, Physica C: Superconductivity **282-287**, 85 (1997), ISSN 0921-4534.  
[10] M. v. Zimmermann, A. Vigliante, T. Niemöller, N. Ichikawa, T. Frello, J. Madsen, P. Wochner, S. Uchida, N. H. Andersen, J. M. Tranquada, et al., Europhysics Letters **41**, 629 (1998).

- [11] P. Abbamonte, A. Rusydi, S. Smadici, G. D. Gu, G. A. Sawatzky, and D. L. Feng, *Nature Physics* **1**, 155 (2005).
- [12] T. Valla, A. V. Fedorov, J. Lee, J. C. Davis, and G. D. Gu, *Science* **314**, 1914 (2006).
- [13] J. M. Tranquada, G. D. Gu, M. Hücker, Q. Jie, H.-J. Kang, R. Klingeler, Q. Li, N. Tristan, J. S. Wen, G. Y. Xu, et al., *Phys. Rev. B* **78**, 174529 (2008).
- [14] H. D. Chen, O. Vafek, A. Yazdani, and S. C. Zhang, *Phys. Rev. Lett.* **93**, 187002 (2004).
- [15] E. Berg, E. Fradkin, E.-A. Kim, S. A. Kivelson, V. Oganesyan, J. M. Tranquada, and S. C. Zhang, *Phys. Rev. Lett.* **99**, 127003 (2007).
- [16] E. Berg, E. Fradkin, and S. A. Kivelson, *Phys. Rev. B* **79**, 064515 (2009).
- [17] Y. Kim and P. Hor, *Modern Physics Letters B* **15**, 497 (2001).
- [18] Y. Kim and P. Hor, *Modern Physics Letters B* **20**, 571 (2006).
- [19] O. Lübben, L. Dudy, A. Krapf, C. Janowitz, and R. Manzke, *Phys. Rev. B* **81**, 174112 (2010).
- [20] K. Zhang, G. Seidler, B. H. Ma, and C. U. Segre, *Physica C* **179**, 405 (1991).
- [21] A. Ariffin, C. Janowitz, B. Müller, L. Dudy, P. Sippel, R. Mitdank, H. Dwelk, A. Krapf, and R. Manzke, *Journal of Physics: Conference Series* **150**, 052084 (2009).
- [22] M. Schneider, R. S. Unger, R. Mitdank, R. Müller, A. Krapf, S. Rogaschewski, H. Dwelk, C. Janowitz, and R. Manzke, *Phys. Rev. B* **72**, 014504 (2005).
- [23] J. Heckel and P. Jugelt, *X-Ray Spectrometry* **13**, 159 (1984).
- [24] Y. Ando, Y. Hanaki, S. Ono, T. Murayama, K. Segawa, N. Miyamoto, and S. Komiyama, *Phys. Rev. B* **61**, R14956 (2000).
- [25] H. Kanai, J. Mizusaki, H. Tagawa, S. Hoshiyama, K. Hirano, K. Fujita, M. Tezuka, and T. Hashimoto, *Journ. Solid State Chem.* **131**, 150 (1997).
- [26] B. Müller, A. Ariffin, R. Mitdank, L. Dudy, J. Rasch, B. Ziegler, L. Lasogga, A. Krapf, C. Janowitz, and R. Manzke, to be published (2010).
- [27] M. Suzuki and M. Hikita, *Phys. Rev. B* **44**, 249 (1991).
- [28] T. Kimura, K. Kishio, T. Kobayashi, Y. Nakayama, N. Motohira, K. Kitazawa, and K. Yamafuji, *Physica C* **192**, 247 (1992).
- [29] Y. Nakamura and S. Uchida, *Phys. Rev. B* **47**, 8369 (1993).
- [30] P. G. Radaelli, D. G. Hinks, A. W. Mitchell, B. A. Hunter, J. L. Wagner, B. Dabrowski, K. G. Vandervoort, H. K. Viswanathan, and J. D. Jorgensen, *Phys. Rev. B* **49**, 4163 (1994).
- [31] T. Shibauchi, H. Kitano, K. Uchinokura, A. Maeda, T. Kimura, and K. Kishio, *Phys. Rev. Lett.* **72**, 2263 (1994).
- [32] Y. Fukuzumi, K. Mizuhashi, K. Takenaka, and S. Uchida, *Phys. Rev. Lett.* **76**, 684 (1996).
- [33] T. Sasagawa, Y. Togawa, J. Shimoyama, A. Kapitulnik, K. Kitazawa, and K. Kishio, *Phys. Rev. B* **61**, 1610 (2000).
- [34] J. Hofer, T. Schneider, J. M. Singer, M. Willemin, H. Keller, T. Sasagawa, K. Kishio, K. Conder, and J. Karpinski, *Phys. Rev. B* **62**, 631 (2000).
- [35] T. Matsuzakia, M. Ido, N. Momonoa, R. M. Dipasupila, T. Nagataa, A. Sakaib, and M. Oda, *Journ. of Phys. and Chem. of Solids* **62**, 29 (2001).
- [36] O. Yuli, I. Asulin, O. Millo, and G. Koren, *Phys. Rev. B* **75**, 184521 (2007).
- [37] H. F. Poulsen, N. H. Andersen, J. V. Andersen, H. Bohr, and O. G. Mouritsen, *Nature* **349**, 594 (1991).
- [38] K. Segawa and Y. Ando, *Phys. Rev. Lett.* **86**, 4907 (2001).
- [39] S.-W. Cheong, G. Aeppli, T. E. Mason, H. Mook, S. M. Hayden, P. C. Canfield, Z. Fisk, K. N. Clausen, and J. L. Martinez, *Phys. Rev. Lett.* **67**, 1791 (1991).
- [40] J. Orenstein and A. J. Millis, *Science* **288**, 468 (2000).
- [41] J. Zaanen and O. Gunnarsson, *Phys. Rev. B* **40**, 7391 (1989).
- [42] V. J. Emery, S. A. Kivelson, and O. Zachar, *Phys. Rev. B* **56**, 6120 (1997).
- [43] Ø. Fischer, M. Kugler, I. Maggio-Aprile, C. Berthod, and C. Renner, *Rev. Mod. Phys.* **79**, 353 (2007).
- [44] S. Fratini and J. Merino, *Phys. Rev. B* **80**, 165110 (2009).
- [45] A. Amaricci, A. Camjayi, K. Haule, G. Kotliar, D. Tanaskovi, and V. Dobrosavljević, *Phys. Rev. B* **82**, 155102 (2010).
- [46] L. Cândido, P. Phillips, and D. M. Ceperley, *Phys. Rev. Lett.* **86**, 492 (2001).
- [47] J. Röhler, *Int. J. Mod. Phys. B* **19**, 255 (2005).
- [48] D. C. Peets, D. G. Hawthorn, K. M. Shen, Y.-J. Kim, D. S. Ellis, H. Zhang, S. Komiyama, Y. Ando, G. A. Sawatzky, R. Liang, et al., *Phys. Rev. Lett.* **103**, 087402 (2009).
- [49] Q. Li, M. Hücker, G. D. Gu, A. M. Tsvelik, and J. M. Tranquada, *Phys. Rev. Lett.* **99**, 067001 (2007).
- [50] A. A. Schafgans, A. D. LaForge, S. V. Dordevic, M. M. Qazilbash, W. J. Padilla, K. S. Burch, Z. Q. Li, S. Komiyama, Y. Ando, and D. N. Basov, *Physical Review Letters* **104**, 157002 (2010).
- [51] K. Yamada, C. H. Lee, K. Kurahashi, J. Wada, S. Wakimoto, S. Ueki, H. Kimura, Y. Endoh, S. Hosoya, G. Shirane, et al., *Phys. Rev. B* **57**, 6165 (1998).